ARMY RESEARCH LABORATORY

Simulation of Error in Optical Radar Range Measurements

by Sandor Der, Brian Redman, and Rama Chellappa

ARL-TR-1488 January 1998

Army Research Laboratory
Adelphi, MD 20783-1197

ARL-TR-1488 **January 1998**

Simulation of Error in Optical Radar Range Measurements

Sandor Der
Sensors and Electron Devices Directorate, ARL

Brian Redman
Communications-Electronics Command

Rama Chellappa
University of Maryland

Abstract

We describe a computer simulation of atmospheric and target effects on the accuracy of range measurements using pulsed laser radars (ladar) with PIN or avalanche photodiodes for direct detection. The computer simulation produces simulated range images as a function of a wide variety of environmental, target, and sensor parameters for ladar with range accuracies smaller than the pulse width. The simulation allows arbitrary target geometries, and simulates speckle, turbulence, and near- and far-field effects. We compare simulation results to actual range error data collected in field tests.

Contents

Figures

Tables

1. Introduction

Laser radar (ladar) is being used increasingly to locate and recognize objects in both industrial and military applications. Recognition algorithms often rely on the range measurements produced by ladar rather than on intensity measurements, because 3-D range imagery usually contains more information than the intensity images, which typically contain large amounts of speckle and noise. Being able to estimate the range error of a ladar configuration is desirable to help choose the design parameters of a ladar and to help design the recognition algorithm. A number of papers address the problem of estimating the probability of detection of laser returns and the probability density functions (pdf's) of range error based on signal-to-noise ratio or carrier-to-noise ratio [1], but these papers generally assume a simple target geometry (e.g., a plane perpendicular to the line of sight) that allows analytic expressions to be derived. The formulas for arbitrarily complex target geometries cannot be solved analytically, but require a numerical solution that would be more computationally complex than the simulation described in this paper. Quantitative analysis is complicated by nonplanar target geometry, laser speckle, and atmospheric scintillation effects, requiring a simulation to be used instead of analytically derived expressions.

The computer simulation that we describe herein produces simulated range images for a direct detection pulse ladar under a wide variety of conditions. The simulation incorporates established theory at each stage. The simulation process is divided into six stages: component disassembly, speckle modulation, scintillation modulation, signal assembly, receiver noise, and pulse detection.

We conducted a field test to collect data to compare with the simulation results. In the field test, we used two flat plywood panels painted carc green as targets. The range measurements we collected using these targets were compared to simulation results to assess the accuracy of the simulation. We intentionally chose a simple target geometry for the field test so that analytical methods could also be used to predict performance for comparison to the simulation results.

2. Laser Simulation

2.1 Component Disassembly

To simulate the effects of target shape, speckle, and scintillation, we decomposed the laser pulse into components along the range and the two crossrange dimensions. Thus the pulse can be expressed as $U(x, y, z)$, where x and y are the horizontal and vertical crossrange dimensions, and z is the range dimension (the direction that the pulse is traveling). The beam's irradiance profile is assumed to be Gaussian, and the pulse shape in the z dimension is an input to the model and can be written as $V(z)$, or alternatively as $V(ct)$, where c is the speed of light and t is time. So we decomposed the outgoing pulse as

$$U(x, y, z) = P_s G(x, y) V(z), \tag{1}$$

where P_s is the total pulse power; x, y, and z take on discrete values; $G(x, y)$ is the proportion of energy within a component located at (x, y) under the two-dimensional Gaussian curve at (x, y); and $V(z)$ is the discrete pulse shape in the range dimension shown in figure 1. The integrals of $G(x, y)$ and $V(z)$ are both one because they are normalized to unity.

Each crossrange component (x, y) corresponds to the energy in a 5- $\times$ 5-cm square area (this size can be set arbitrarily, of course) at target range; thus, the number of crossrange components that the simulation uses depends on the range and the beam divergence of the sensor. In table 1 we show the portion of energy in each crossrange component for a pulse that spreads to an area of 25 $\times$ 25 cm at target range. The distance that each component travels is determined by a geometric model, which is an input to the simulation, and has resolution of 5 $\times$ 5 cm, matching the crossrange decomposition of the pulse. At the target, each component is treated as if it encounters a resolved planar surface perpendicular to the line of sight to the sensor. However, a pulse may see nonperpendicular surfaces and unresolved surfaces as a set of components at differing ranges. The pulses are not split by frequency because we assume a quasi-monochromatic source. For a broadband source, such as a semiconductor laser, accurate modeling of speckle would require either breaking up the pulses by frequency, or using a different distribution than the one we use to model speckle and turbulence modulation.

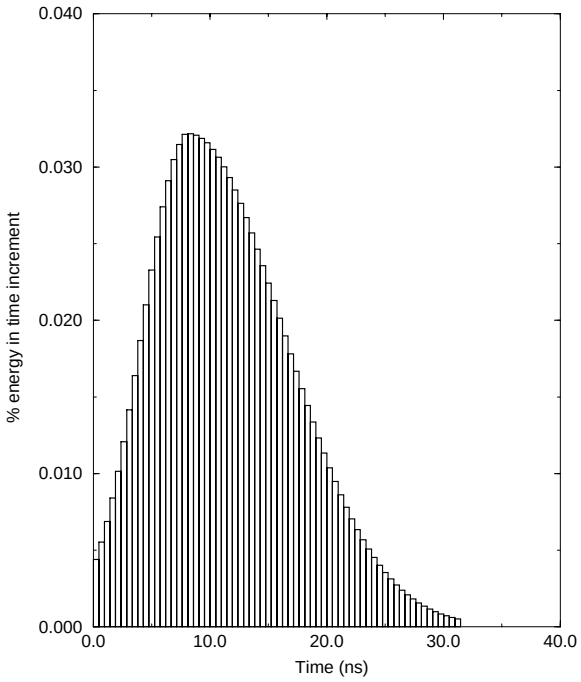

Figure 1. Simulated laser pulse shape.

Table 1. Portion of total pulse energy in crossrange components with Gaussian irradiance profile *($G(x, y)$)*.

Location	x = –0.1	x = –0.05	x = 0.0	x = 0.05	x = 0.1
y = 0.1	0.003	0.014	0.022	0.014	0.003
y = 0.05	0.014	0.059	0.095	0.059	0.014
y = 0.0	0.022	0.095	0.154	0.095	0.022
y = –0.05	0.014	0.059	0.095	0.059	0.014
y = –0.1	0.003	0.014	0.022	0.014	0.003

The standard radar equation governs the return power received for each component sent [1]. Therefore, the received component power is given by

$$P_R = P_c e^{-2\alpha R} \frac{d^2}{4R^2} \epsilon \rho, \tag{2}$$

where P_R is the received component power, P_c is the transmitted component power, α is the atmospheric extinction coefficient, R is the range to the target, d is the effective diameter of the receiver's clear aperture, ϵ is the receiver's optical efficiency, and ρ is the diffuse reflectivity of the resolved

target. The resolved target assumption is applied only at the level of the component; the pulse itself may be unresolved.

2.2 Speckle and Turbulence Modulation

The power received from each component is modulated by speckle and turbulence. Speckle is applied to each component with the use of the exponential distribution to modulate the received power, because we assume a quasi-monochromatic source. For broadband sources, the method described by Parry [2] could be used to compute the pdf. Thus, the power received from a component in the presence of speckle is

$$P_{speckle} = S(P_R), \tag{3}$$

where S is an exponentially distributed random variable with parameter P_R,

$$Prob[S(\lambda) = s] = \frac{e^{\frac{-s}{\lambda}}}{\lambda}, \tag{4}$$

where λ is the mean of the exponential random variable [3]. Similarly, turbulence is applied by modulating the power of each component with a lognormal random variable. Some authors have argued that other distributions for turbulence are more appropriate, especially in high turbulence in which the K distribution matches the data well [4], although it tends to underestimate probabilities of high irradiances [5]. Experimental evidence suggests that in the presence of significant aperture averaging, the statistics of the irradiance are lognormal even in the high-fluctuation regime [6]. Many other pdf's have been suggested, but none have been shown to fit the data under all conditions [5]. The simulation uses modular code, making the pdf easy to change if consensus is reached. The mean μ of the variable is the power before the application of the turbulence. We determine the mean normalized variance σ_I^2 by [7]

$$\sigma_I^2 = \gamma_{target}\sigma_{Ipoint}^2, \tag{5}$$

where the term γ_{target} accounts for the target averaging of turbulence, σ_{Ipoint}^2 is the intensity fluctuation for a point target without aperture averaging, and

$$\sigma_{Ipoint}^2 = 1.23c_n^2(k)^{\frac{7}{6}}(2R)^{\frac{11}{6}}, \tag{6}$$

where R is the range from the target to the sensor, k is the wave number, and c_n^2 is the turbulence refractive index structure constant, which is dependent on atmospheric conditions. The value of c_n^2 used in the simulation is a

user controlled input parameter. We obtained typical values from Shapiro *et al* [1] and determined the target averaging term γ_{target} by [7]

$$\gamma_{target} = \left(\frac{\rho_l}{r_{eff}}\right)^{\frac{7}{3}}, \tag{7}$$

where the value

$$r_{eff} = \min[r_{tgt}, r_{beam}(R), r_{fov}(R)] \tag{8}$$

is a measure of the effective averaging area and ρ_l is the long-term turbulence cell size. We calculated the ρ_l using

$$\rho_l = \frac{\sqrt{\frac{R}{k}}}{\sqrt{1 + \frac{R}{k{\rho_0}^2}}}, \tag{9}$$

where [7]

$$\rho_0 = \rho_0^{(p)} \left[\frac{(1 - \frac{R}{f_{xmt}})^2 + (\frac{R}{z_B})^2 (1 + \frac{\delta^2}{3}) \frac{1}{1+\delta^2}}{1 - \frac{13}{3}(\frac{R}{f_{xmt}}) + \frac{11}{3}(\frac{R}{f_{xmt}})^2 + \frac{1}{3}(\frac{R}{z_B})^2 \frac{(1+\frac{\delta^2}{4})}{(1+\delta^2)}} \right]^{\frac{1}{2}}, \tag{10}$$

$$\rho_0^{(s)} = (0.5k^2 c_n^2 R)^{\frac{-3}{5}}, \tag{11}$$

$$\rho_0^{(p)} = (1.46k^2 c_n^2 R)^{\frac{-3}{5}}, \tag{12}$$

$$z_B = (\frac{kr_{bo}}{2}) \left[\frac{1}{(\rho_0^{(s)})^2} + \frac{1}{4r_{bo}^2} \right]^{\frac{-1}{2}}, \tag{13}$$

$$f_{xmt} = \frac{-r_{b0}}{\tan(\theta_{b1/2}) - \tan(\frac{\lambda}{2\pi r_{b0}})}, \tag{14}$$

$$\delta = \frac{2r_{b0}}{\rho_0^{(p)}}. \tag{15}$$

The Rytov solution (eq 5) predicts that the variance of the intensity fluctuation increases indefinitely as range or the structure constant c_n^2 increases. Empirical measurements show that the normalized variance of intensity fluctuations saturate at approximately 1, whereas the normalized irradiance variance is unbounded in the Rytov solution [8]. The empirical curve of this saturation is shown in figure 2. This curve is stored as a lookup table in the simulation.

The received power in a component after turbulence is then

$$P_{turbulence} = e^{G(a,b)} P_{speckle}, \tag{16}$$

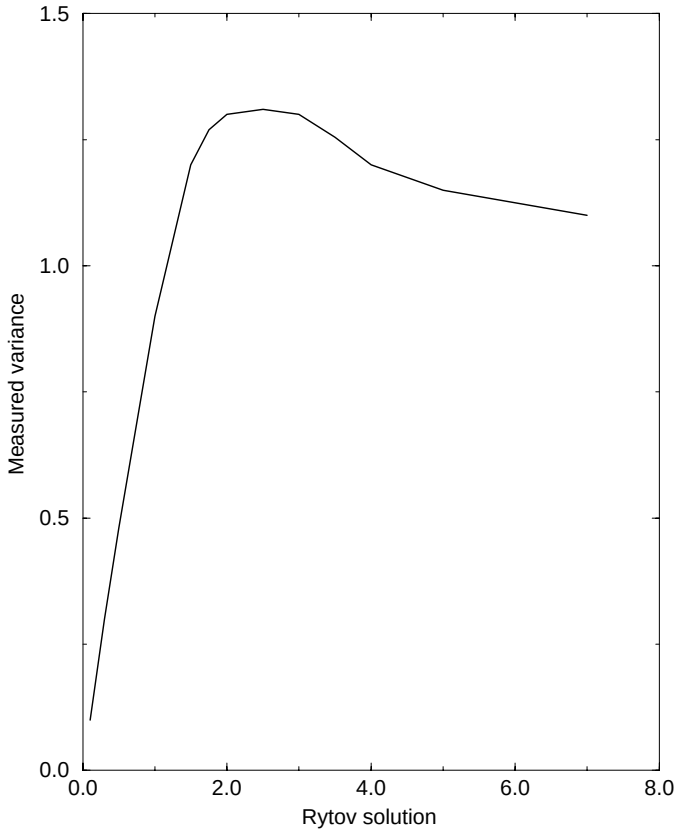

Figure 2. Saturation of intensity fluctuation.

where G is a Gaussian random variable with mean a and variance b. We determined the parameters a and b from the mean and variance of the log-normal distribution using

$$b = \sqrt{\log(\frac{\sigma^2}{\mu e^2 + 1})}, \tag{17}$$

$$a = \log(\mu) - \frac{b^2}{2}. \tag{18}$$

The speckle and turbulence modulation of the component intensities is not independent from component to component. The correlation length of the speckle and turbulence in the crossrange dimension are calculated, and components are grouped together so that the combined components are the size of a turbulence or speckle cell. The turbulence cell size is equivalent to the value ρ_l calculated in equation (9). The speckle cell size in the

target plane is

$$l_{speckle} = \frac{\lambda R}{\sqrt{A_o}}, \tag{19}$$

where A_o is the area of the receiver optics. The correlation time of speckle and turbulence for a single path is assumed to be greater than the pulse width, so that turbulence and speckle for a given pulse is a function only of crossrange dimensions (x, y), not of the range dimension z.

Once we applied speckle and turbulence, we summed the components in the crossrange dimension to form the return signal at the detector. Each component is shifted in range corresponding to the range to the target for that component. The returning power at the detector then has the form

$$U_r(z) = \sum_{x,y} P_{turbulence}(x, y) V(z - 2T(x, y)), \tag{20}$$

where the crossrange dependence of $P_{turbulence}(x, y)$ is made explicit, and $T(x, y)$ represents the range to the target at location (x, y).

2.3 Detector and Amplifier Noise

The return signal power is multiplied by ξ_{ann}, which is a function of the geometric radius of the laser spot image, turbulence blur circle, and diffraction limited blur radius. We then calculated the factor as [9]

$$\xi_{ann} = \frac{2\pi F_{gc}(R)}{\pi r_b^2(R)} \int_0^{r_b(R)} \xi_a(R, r) r dr, \tag{21}$$

$$\xi_a(R, r) = \frac{\Lambda(r_D, \frac{r_{aper} f_{rcvr}}{R}, \frac{r f_{rcvr}}{R}) - \Lambda(r_D, \frac{r_{obs} f_{rcvr}}{R}, \frac{r f}{R})}{\pi(\frac{r_{aper} f_{rcvr}}{R})^2}, \tag{22}$$

$$\Lambda(a, b, c) \doteq b^2 \Psi(a, b, c) + a^2 \Psi(b, a, c) - ac \sin(\Psi(b, a, c)), \tag{23}$$

$$\Psi(b, a, c) \doteq \arccos\Big(\frac{c^2 + b^2 - a^2}{2bc}\Big), \tag{24}$$

$$F_{gc}(R) = \min\Big(\frac{A_d}{A_{blur}(R)}, 1\Big), \tag{25}$$

where A_d is the area of the detector, r_{aper} is the radius of the receiver aperture, r_{obs} is the radius of the obscuration, $F_{gc}(R)$ is the detector geometric compression factor, and

$$A_{blur}(R) = \pi r_{blur}(R)^2, \tag{26}$$

$$r_{blur}(R) = r_{geom}(R) + r_{turb+diff}(R). \tag{27}$$

The diffraction limited blur radius and turbulence blur circle radius for the short exposure case can be taken as

$$r_{turb+diff} = r_{diff}\Big[1 + \frac{r_{diff}}{r_{trb}}^2\Big]^{-\frac{1}{2}}, \tag{28}$$

$$r_{diff} = \frac{1.22\lambda f_{rcvr} Q}{d_{rcv}}, \tag{29}$$

$$r_{turb} = \frac{2}{\pi \nu_{trb}}, \tag{30}$$

where ν_{trb} is the turbulence cutoff spatial frequency given by the solution ν of the equation [10]

$$(\frac{1}{3.44})^{\frac{3}{5}}(\frac{r_0}{\lambda f_{rcvr}}) = \nu\Big[1 - \alpha(\frac{\lambda f_{rcvr}\nu}{d_{rcv}})^{\frac{1}{3}}\Big]^{\frac{3}{5}} \tag{31}$$

and

$$r_0 = 2.1(1.46k^2 c_n^2 R)^{-\frac{3}{5}} \tag{32}$$

is Fried's coherent aperture diameter because of turbulence. The geometric radius of the laser spot image is

$$r_{geom} = \frac{f_{rcvr}}{R} r_b(R), \tag{33}$$

where the laser spot radius $r_b(R)$ is calculated as [11]

$$r_b(R) = \Big[\frac{R^2}{k^2 r_{b0}^2} + r_{b0}^2(1 - \frac{R}{f_{xmt}})^2 + \frac{4R^2}{k^2\rho_l^2}\Big]^{\frac{1}{2}}, \tag{34}$$

if $R > k\min(\rho_l^2, 4r_{b0}^2)$ or $\rho_l > 2r_{b0}$, and

$$r_b(R) = \left\{\frac{R^2}{k^2 r_{b0}^2} + r_{b0}^2(1 - \frac{R}{f_{xmt}})^2 + \frac{4R^2}{k^2\rho_l^2}\Big[1 - 0.62\Big(\frac{\rho_l}{2r_{b0}}\Big)^{\frac{1}{3}}\Big]^{\frac{6}{5}}\right\}^{\frac{1}{2}}, \tag{35}$$

$$f_{xmt} = \frac{-r_{b0}}{\tan(\theta_{b1/2}) - \tan(\frac{\lambda}{2\pi r_{b0}})}, \tag{36}$$

otherwise. In equations (31) to (36), r_{b0} is the radius of the beam waist, f_{rcvr} is the focal length of the receiver, f_{xmt} is the effective focal length of the transmitter, $\theta_{b1/2}$ is the half-angle transmitted beam divergence, Q is the quality factor of the optics, d_{rcv} is the diameter of the effective clear aperture, λ is the wavelength of the laser, k is the wave number, and R is the range to the target.

The return signal is subject to background noise, shot noise, amplifier noise, and dark current noise, all of which are independent, identically distributed (iid) Gaussian. The detector noise, consisting of dark, shot, and background noise, is calculated as [12]

$$NEP_{Detector} = \frac{\sqrt{2e_c B[I_{ds} + (I_{db} + I_b + I_s)M^2 F]}}{\mathcal{R}}, \tag{37}$$

where $\mathcal{R}$ is the responsivity of the detector, B is the electrical bandwidth, I_{ds} is the surface dark current, I_{db} is the bulk dark current at unity gain, $I_b = \mathcal{R}P_B$ is the current because of the background illumination, $I_s = \mathcal{R}P_{turbulence}$ is the current because of the received signal, M is the detector gain, and F is the excess noise factor because of the detector gain. P_B is the background power calculated from

$$P_B = \rho h_{sun} T_r A_r \sin\Big(\frac{\theta_{fov}}{2}\Big)^2 \Delta\lambda, \tag{38}$$

where A_r is the area of the receiver, T_r is the transmission of the receiver, ρ is the background reflectance, θ_{fov} is the field of view, h_{sun} is the background solar irradiance, and $\Delta\lambda$ is the optical bandwidth.

Amplifier noise is calculated assuming a basic RC filtered amp. It follows

$$NEP_{Amp} = \sqrt{\frac{4kTBN}{R_L \mathcal{R}^2}}, \tag{39}$$

where k is Boltzmann's constant, T is the temperature in Kelvins, B is the electrical bandwidth, N is the noise factor for the electronics, and R_L is the load resistor calculated from

$$R_L = \frac{1}{2\pi BC}, \tag{40}$$

where C is the capacitance of the detector.

The noises are added in quadrature to determine the overall noise figure for the detectors

$$NEP_{Total} = \sqrt{NEP_{Amp}^2 + NEP_{Detector}^2}\,. \tag{41}$$

The NEP is the standard deviation of the Gaussian distribution of the additive noise in the optical power domain. The simulation generates a Gaussian random variable with zero mean and a standard deviation equal to NEP. This Gaussian noise is added to the signal, and then is filtered according to the electrical bandwidth of the sensor. The noisy signal is then passed to the pulse detector.

The pulse detection portion of the simulation is modifed according to the sensor being simulated. Commonly used pulse detection algorithms include matched filtering followed by peak detection, threshold detection of the rising edge of the pulse, or detection averaging of the rising and falling edge of the pulse. Quantization error of the system clock is simulated by shifting the transmitted and received pulse by a random variable that is uniformly distributed across $\pm$ one-half of a clock cycle.

Figure 3 shows the effect of the noise on the simulated received pulse. Figure 4 shows a simulated ladar range image exhibiting the effects of the signal fluctuations and noise included in the simulation.

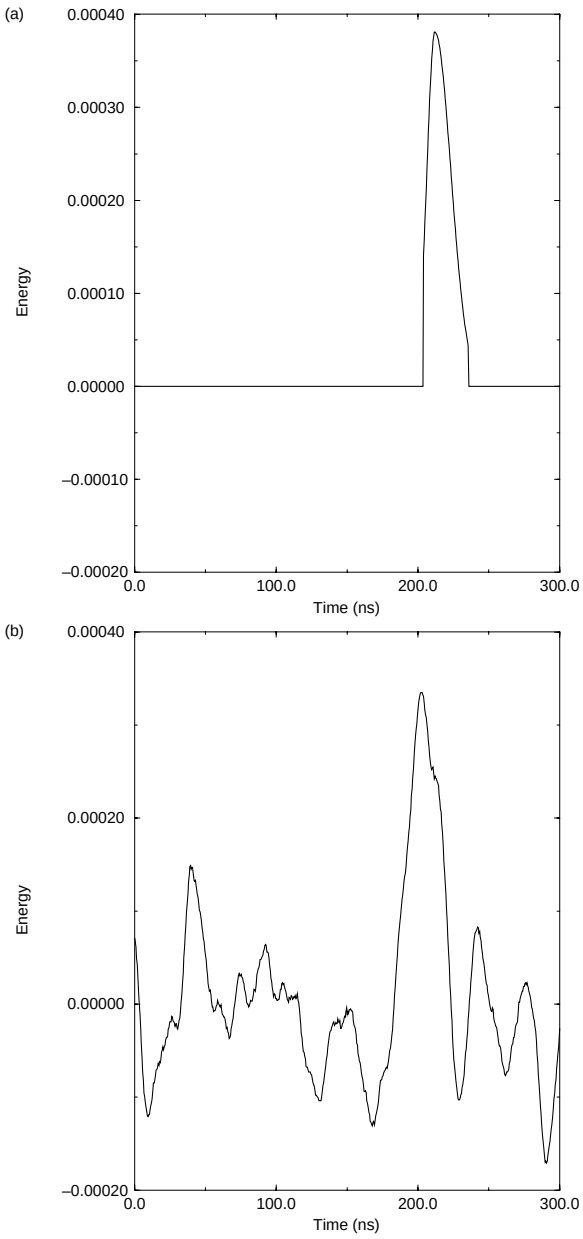

Figure 3. Simulated received pulse: (a) undistorted pulse shape, signal without noise, and (b) noisy return signal after matched filtering.

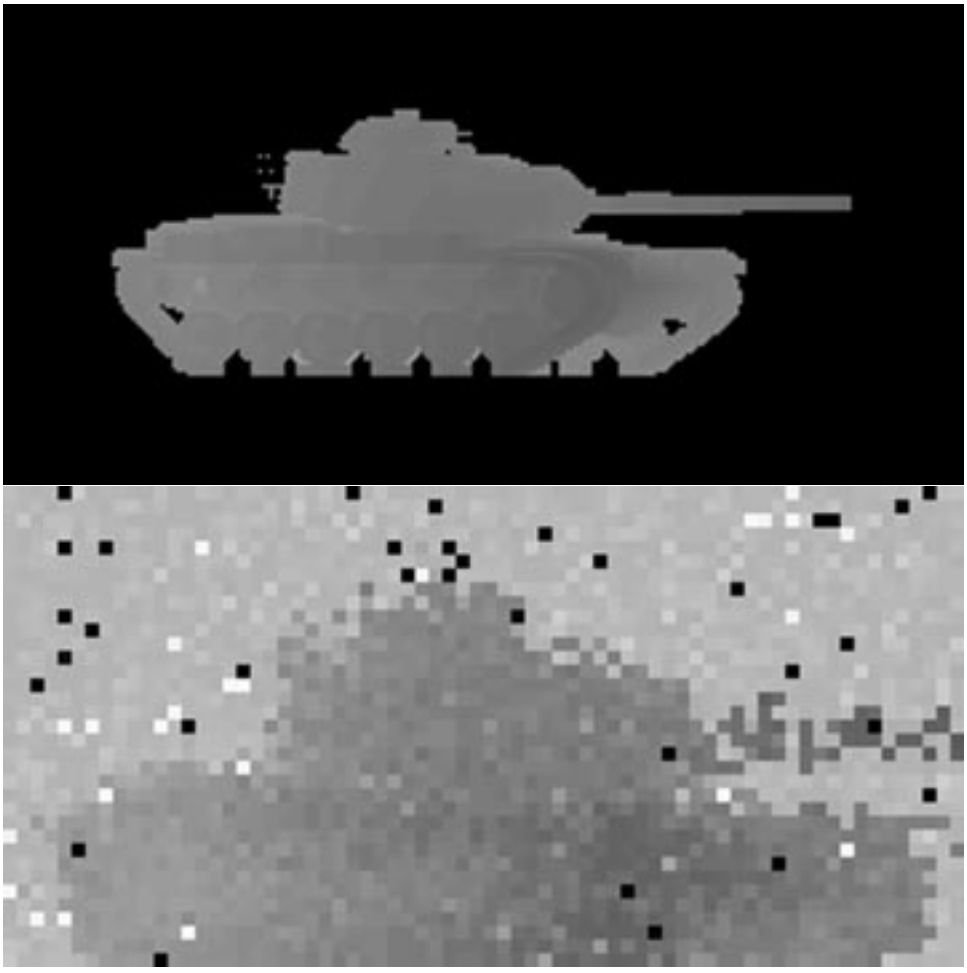

Figure 4. Input range image and resulting ladar image. (Black pixels indicate dropouts and white pixels indicate anomalies.)

3. Comparison of Simulated Data to Real Data

As a check on the quality of the simulation, we gathered a small amount of real data. We painted a 4- $\times$ 8-ft sheet of plywood carc green and positioned it perpendicular to the line of sight to the sensor. We captured ladar images of the plywood and extracted an empirical pdf from the images. Figure 5 shows simulated range error as a function of range. The two x's mark the range's standard deviation for the real ladar. Additional simulation runs showed that the ladar is clock quantization error limited at short ranges and signal-to-noise ratio limited at longer ranges. Many ladar systems, including the Lockheed Martin Vought system, avoid the sharp increase in error at longer ranges by returning no range value for return pulses that do not exceed several times the ambient root mean square (rms) noise level. Such a return pulse is called a dropout. The percentage of dropout pixels would then increase as range increases, while the range error on nondropout pixels would increase much more slowly. Table 2 gives a partial list of sensor parameters.

The plywood target data that we collected have characteristics that limit validation uses. The Lockheed Martin Vought ladar has a relatively large aperture, so aperture averaging makes the effects of speckle and scintillation almost negligible. The detector noises are dominated by amplifier noise, so background and shot noise effects are not adequately tested. While the comparison of real and simulated data was useful in validating the simulation, it is far from thorough. A thorough empirical validation would require laser systems having at least several different values of each sensor parameter, so that each sensor parameter is accurately modeled.

To test the speckle and scintillation portion of the simulation, we had to reduce the aperture size until aperture averaging was insufficient to make speckle and scintillation effects negligible. The aperture size was reduced while the output power of the laser was increased so that average return power remained a constant; thus the primary cause of variation in performance is the reduction in aperture averaging that occurs at smaller aperture sizes. Figure 6 shows the resulting simulated performance.

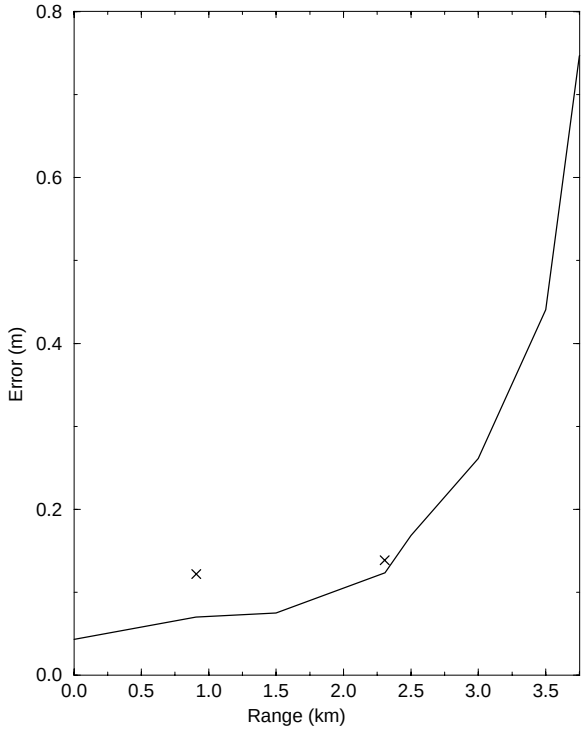

Figure 5. Simulated range error versus range (x's mark real data points).

Table 2. Sensor description.

Parameter	Value
Laser type	Nd:YAG
Wavelength	1.574 μm
Beam divergence	125 μrad
Pulse width	10 ns
Pulse energy	250 μJ

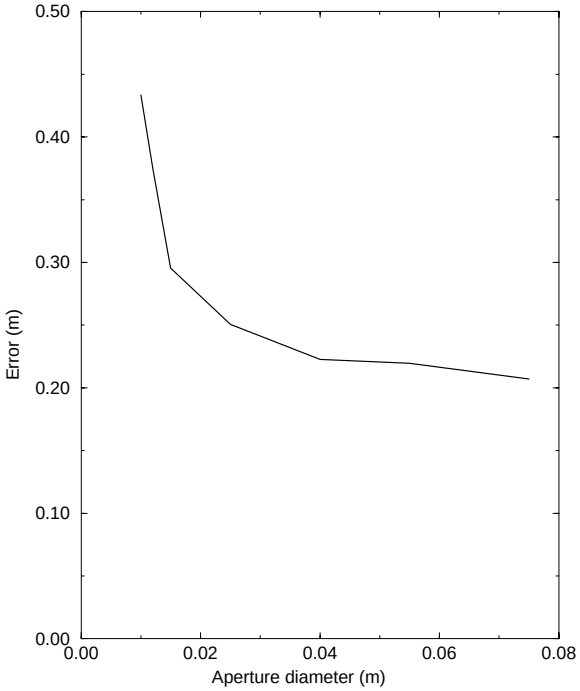

Figure 6. Simulated range error versus aperture size. (Laser power was varied to keep average return power constant. Speckle correlation cell diameter was 0.015 m.)

4. Conclusions

We have described a computer simulation that estimates ladar range performance as a function of sensor, environmental, and target parameters. By breaking the pulse into components, the simulation is able to simulate laser returns for arbitrary target geometries.

Comparison of simulated data to a limited set of real data shows a close match. Unfortunately, we were unable to collect a wider variety of data, such as data at longer ranges. Additional data validation is needed.

The simulation has been used in performance versus cost trade-off studies during the design phase of the Communications-Electronics Command (CECOM) Multifunction Laser System (MFLS). Currently, it is being used to estimate range error as an aid to designing ladar automatic target recognizer algorithms in a joint program at CECOM and the Army Research Laboratory (ARL).

Acknowledgments

The authors would like to thank David DuBois, Bruno Evans, Kim Jenkins, Don Nimblett, and James Tomlin of Lockheed Martin Vought Systems for their support in providing the ladar for gathering and acquiring the data.

References

1. J. Shapiro, B. Capron, and R. Harney, "Imaging and target detection with a heterodyne-reception optical radar," Appl. Op. **20**, 3292–3313, October 1981.

2. G. Parry, "Speckle patterns in partially coherent light," *Laser Speckle and Related Phenomena*, J. Dainty, ed., New York: Springer Verlag, 1985.

3. J. Goodman, "Statistical Properties of Laser Speckle Patterns," *Laser Speckle and Related Phenomena*, J. Dainty, ed., New York: Springer Verlag, 1985.

4. G. Parry, "Measurement of atmospheric turbulence induced intensity fluctuations in a laser beam," OPTICA ACTA **28**, No. 5, 715–728, 1981.

5. J. Churnside and S. Clifford, "Log-normal Rician probability-density function of optical scintillations in the turbulent atmosphere," J. Opt. Soc. Am. A **4**, No. 10, 1923–1930, October 1987.

6. R. DeWitt, "The distribution of irradiance fluctuations that result from atmospheric turbulence," PSR Note N406, Pacific Sierra Research Corporation, 1456 Cloverfield Blvd., Santa Monica, CA 90404, August 1981.

7. R. Lutomirski, R. Huschke, W. Meecham, and H. Yura, "Degradation of laser systems by atmospheric turbulence," Defense Advanced Research Projects Agency, R-9171-ARPA / RC, 3701 North Fairfax Drive, Arlington, VA, 22203-1714, June 1973.

8. A. Ishimaru, *Wave Propagation and Scattering in Random Media* **2**, New York: Academic Press, 1978.

9. R. Measures, *Laser Remote Sensing, Fundamentals and Applications*, John Wiley and Sons, 1984.

10. J. Goodman, *Statistical Optics*, New York: Wiley, 1985.

11. R. Fante, "Electromagnetic beam propagation in turbulent media," Proceedings of the IEEE **63**, No. 12, 1669–1693, December 1975.

12. P. Webb, R. McIntyre, and J. Conradi, “Properties of avalanche photodiodes,” RCA Review **35**, 234–278, June 1974.

Distribution

Admnstr
Defns Techl Info Ctr
Attn DTIC-OCP
8725 John J Kingman Rd Ste 0944
FT Belvoir VA 22060-6218

Ofc of the Dir Rsrch and Engrg
Attn R Menz
Pentagon Rm 3E1089
Washington DC 20301-3080

Ofc of the Secy of Defns
Attn ODDRE (R&AT) G Singley
Attn ODDRE (R&AT) S Gontarek
The Pentagon
Washington DC 20301-3080

OSD
Attn OUSD(A&T)/ODDDR&E(R) J Lupo
Washington DC 20301-7100

CECOM
Attn PM GPS COL S Young
FT Monmouth NJ 07703

CECOM RDEC Elect System Div Dir
Attn J Niemela
FT Monmouth NJ 07703

CECOM
Sp & Terrestrial Commctn Div
Attn AMSEL-RD-ST-MC-M H Soicher
FT Monmouth NJ 07703-5203

Dept of the Army (OASA) RDA
Attn SARD-PT R Saunders
103 Army
Washington DC 20301-0103

Dir of Assessment and Eval
Attn SARD-ZD H K Fallin Jr
103 Army Pentagon Rm 2E673
Washington DC 20301-0163

Hdqtrs Dept of the Army
Attn DAMO-FDT D Schmidt
400 Army Pentagon Rm 3C514
Washington DC 20301-0460

MICOM RDEC
Attn AMSMI-RD W C McCorkle
Redstone Arsenal AL 35898-5240

US Army Avn Rsrch, Dev, & Engrg Ctr
Attn T L House
4300 Goodfellow Blvd
St Louis MO 63120-1798

US Army CECOM Rsrch, Dev, & Engrg
Attn R F Giordano
FT Monmouth NJ 07703-5201

US Army Edgewood Rsrch, Dev, & Engrg Ctr
Attn SCBRD-TD J Vervier
Aberdeen Proving Ground MD 21010-5423

US Army Info Sys Engrg Cmnd
Attn ASQB-OTD F Jenia
FT Huachuca AZ 85613-5300

US Army Materiel Sys Analysis Agency
Attn AMXSY-D J McCarthy
Aberdeen Proving Ground MD 21005-5071

US Army Matl Cmnd
Dpty CG for RDE Hdqtrs
Attn AMCRD BG Beauchamp
5001 Eisenhower Ave
Alexandria VA 22333-0001

US Army Matl Cmnd
Prin Dpty for Acquisition Hdqrts
Attn AMCDCG-A D Adams
5001 Eisenhower Ave
Alexandria VA 22333-0001

US Army Matl Cmnd
Prin Dpty for Techlgy Hdqrts
Attn AMCDCG-T M Fisette
5001 Eisenhower Ave
Alexandria VA 22333-0001

US Army Natick Rsrch, Dev, & Engrg Ctr
Acting Techl Dir
Attn SSCNC-T P Brandler
Natick MA 01760-5002

Distribution

US Army NVESD
Attn AMSRL-RD-NV-UAB C Walters
10221 Burbeck Rd Ste 40
FT Belvoir VA 22060

US Army Rsrch Ofc
Attn G Iafrate
4300 S Miami Blvd
Research Triangle Park NC 27709

US Army Simulation, Train, & Instrmntn Cmnd
Attn J Stahl
12350 Research Parkway
Orlando FL 32826-3726

US Army Tank-Automtv & Armaments Cmnd
Attn AMSTA-AR-TD C Spinelli
Bldg 1
Picatinny Arsenal NJ 07806-5000

US Army Tank-Automtv Cmnd Rsrch, Dev, & Engrg Ctr
Attn AMSTA-TA J Chapin
Warren MI 48397-5000

US Army Test & Eval Cmnd
Attn R G Pollard III
Aberdeen Proving Ground MD 21005-5055

US Army Train & Doctrine Cmnd
Battle Lab Integration & Techl Dirctrt
Attn ATCD-B J A Klevecz
FT Monroe VA 23651-5850

US Military Academy
Dept of Mathematical Sci
Attn MAJ D Engen
West Point NY 10996

USAASA
Attn MOAS-AI W Parron
9325 Gunston Rd Ste N319
FT Belvoir VA 22060-5582

Nav Surface Warfare Ctr
Attn Code B07 J Pennella
17320 Dahlgren Rd Bldg 1470 Rm 1101
Dahlgren VA 22448-5100

GPS Joint Prog Ofc Dir
Attn COL J Clay
2435 Vela Way Ste 1613
Los Angeles AFB CA 90245-5500

Special Assist to the Wing Cmndr
Attn 50SW/CCX Capt P H Bernstein
300 O'Malley Ave Ste 20
Falcon AFB CO 80912-3020

DARPA
Attn B Kaspar
Attn L Stotts
3701 N Fairfax Dr
Arlington VA 22203-1714

ARL Electromag Group
Attn Campus Mail Code F0250 A Tucker
University of Texas
Austin TX 78712

Univ of Maryland Dept of Elec Engrg
Attn R Chellappa
Rm 2365 A V Williams Bldg
College Park MD 20742-3285

Dir for MANPRINT
Ofc of the Deputy Chief of Staff for Prsnnl
Attn J Hiller
The Pentagon Rm 2C733
Washington DC 20301-0300

ERIM
Attn C Dwan
Attn J Ackenhusen
1975 Green Rd
Ann Arbor MI 48105

Palisades Instit for Rsrch Svc Inc
Attn E Carr
1745 Jefferson Davis Hwy Ste 500
Arlington VA 22202-3402

US Army Rsrch Lab
Attn AMSRL-CI-LL Techl Lib (3 copies)
Attn AMSRL-CS-AL-TA Mail & Records Mgmt

Distribution

US Army Rsrch Lab (cont'd)
Attn AMSRL-CS-AL-TP Techl Pub (3 copies)
Attn AMSRL-SE J M Miller
Attn AMSRL-SE J Pellegrino
Attn AMSRL-SE-EE Z G Sztankay
Attn AMSRL-SE-SE D Nguyen
Attn AMSRL-SE-SE J Phillips
Attn AMSRL-SE-SE L Bennett

US Army Rsrch Lab (cont'd)
Attn AMSRL-SE-SE M Vrabel
Attn AMSRL-SE-SE N Nasrabadi
Attn AMSRL-SE-SE P Rauss
Attn AMSRL-SE-SE S Der (5 copies)
Attn AMSRL-SE-SE T Kipp
Adelphi MD 20783-1197

REPORT DOCUMENTATION PAGE

Form Approved
OMB No. 0704-0188

1. AGENCY USE ONLY *(Leave blank)*	2. REPORT DATE	3. REPORT TYPE AND DATES COVERED
	January 1998	Final, June 1997

4. TITLE AND SUBTITLE
Simulation of Error in Optical Radar Range Measurements

5. FUNDING NUMBERS
PE: 61102A

6. AUTHOR(S)
Sandor Der, Brian Redman, and Rama Chellappa

7. PERFORMING ORGANIZATION NAME(S) AND ADDRESS(ES)
U.S. Army Research Laboratory
Attn: AMSRL-SE-SE (sder@arl.mil)
2800 Powder Mill Road
Adelphi, MD 20783-1197

8. PERFORMING ORGANIZATION REPORT NUMBER
ARL-TR-1488

9. SPONSORING/MONITORING AGENCY NAME(S) AND ADDRESS(ES)
U.S. Army Research Laboratory
2800 Powder Mill Road
Adelphi, MD 20783-1197

10. SPONSORING/MONITORING AGENCY REPORT NUMBER

11. SUPPLEMENTARY NOTES
AMS code: P611102.305
ARL PR: 7NE0M1

12a. DISTRIBUTION/AVAILABILITY STATEMENT
Approved for public release; distribution unlimited.

12b. DISTRIBUTION CODE

13. ABSTRACT *(Maximum 200 words)*

We describe a computer simulation of atmospheric and target effects on the accuracy of range measurements using pulsed laser radars (ladar) with PIN or avalanche photodiodes for direct detection. The computer simulation produces simulated range images as a function of a wide variety of environmental, target, and sensor parameters for ladar with range accuracies smaller than the pulse width. The simulation allows arbitrary target geometries, and simulates speckle, turbulence, and near- and far-field effects. We compare simulation results to actual range error data collected in field tests.

14. SUBJECT TERMS
Pulse laser radar, laser ranging 3-D imaging, range imaging, ladar

15. NUMBER OF PAGES
31

16. PRICE CODE

17. SECURITY CLASSIFICATION OF REPORT	18. SECURITY CLASSIFICATION OF THIS PAGE	19. SECURITY CLASSIFICATION OF ABSTRACT	20. LIMITATION OF ABSTRACT
Unclassified	Unclassified	Unclassified	UL

NSN 7540-01-280-5500

Standard Form 298 (Rev. 2-89)
Prescribed by ANSI Std. Z39-18
298-102

DEPARTMENT OF THE ARMY
U.S. Army Research Laboratory
2800 Powder Mill Road
Adelphi, MD 20783-1197